Kinetically Controlled Formation of Supported Nanoparticles in Low Temperature Supercritical Media for the Development of Advanced Nanostructured Materials

ARTICLE *in* THE JOURNAL OF PHYSICAL CHEMISTRY C · MARCH 2009

Impact Factor: 4.77 · DOI: 10.1021/jp809533n

6 AUTHORS, INCLUDING:

Samuel Marre
Institut de Chimie de la matière condensée…
60 PUBLICATIONS **794** CITATIONS
SEE PROFILE

Arnaud Erriguible
Institut Polytechnique de Bordeaux
22 PUBLICATIONS **211** CITATIONS
SEE PROFILE

Frederic Marias
Université de Pau et des Pays de l'Adour
60 PUBLICATIONS **435** CITATIONS
SEE PROFILE

Cyril Aymonier
French National Centre for Scientific Resea…
137 PUBLICATIONS **2,147** CITATIONS
SEE PROFILE

THE JOURNAL OF PHYSICAL CHEMISTRY C

Article

Kinetically Controlled Formation of Supported Nanoparticles in Low Temperature Supercritical Media for the Development of Advanced Nanostructured Materials

Samuel Marre, Arnaud Erriguible, Arturo Perdomo, Francois Cansell, Frederic Marias, and Cyril Aymonier

J. Phys. Chem. C, **2009**, 113 (13), 5096-5104• DOI: 10.1021/jp809533n • Publication Date (Web): 09 March 2009

Kinetically Controlled Formation of Supported Nanoparticles in Low Temperature Supercritical Media for the Development of Advanced Nanostructured Materials

Samuel Marre,[†] Arnaud Erriguible,[†] Arturo Perdomo,[†] Francois Cansell,[‡] Frederic Marias,[§] and Cyril Aymonier*[,†,‡]

CNRS, Institut de Chimie de la Matière Condensée de Bordeaux, 87 avenue du Docteur Albert Schweitzer, 33608, Pessac Cedex, France, Université de Bordeaux, Institut de Chimie de la Matière Condensée de Bordeaux, ENSCPB, 16 avenue Pey Berland, F33607 Pessac Cedex, France, and Université de Pau et des Pays de l'Adour, Laboratoire thermique Energétique et Procédés, rue Jules Ferry, F64075, Pau, France

Received: October 28, 2008; Revised Manuscript Received: January 28, 2009

The formation of surface nanostructures allows assemblies of materials at different scales, opening new routes toward the design of advanced nanostructured materials. The decoration of surfaces with shape- and size-controlled metal nanoparticles can be achieved through the reduction of hexafluoroacetylacetonate complexes [$M(hfac)_x$] with H_2 in supercritical CO_2/alcohol at low temperature with neither catalyst nor surface prefunctionalization. This paper investigates the influence of different alcohols, methanol, ethanol, and isopropanol, used as cosolvent on the reduction kinetics of $Cu(hfac)_2 \cdot H_20$ in the supercritical CO_2/alcohol/H_2 mixtures. The results are applied to the modeling of the decoration process of silica spheres, used as a model substrate, with copper nanoparticles (5−17 nm). The model, using the decomposition kinetics of the precursor, is based on a bimodal process: (i) an initial homogeneous nucleation in the supercritical media and (ii) a fast heterogeneous growth by coalescence on the surface of the silica particles. We demonstrate good agreements between the simulated results and the experimental data showing an advanced kinetically controlled size of the supported nanoparticles in the range of temperature 100−125 °C and residence time 0−120 min.

1. Introduction

Progress in nanotechnology toward the fabrication of nanodevices now requires the assembly of materials at length scaling from a few nanometers up to thousands of nanometers. This concept allows the development of advanced nanostructured materials, which have attracted wide interest in view of the new properties that can be developed, taking advantage of the association of several materials at the nanometer scale (quantum confinement or high surface to volume ratio).[1] In this purpose, more and more studies are nowadays focused on the control of materials properties via modification of their surface.[2] A particularly interesting challenge stands in combining properties of materials at different scales (from bulk properties down to size-dependent properties) via the deposition of nano-objects with controlled size and shape on surfaces of bulk materials (supported nanoparticles). These supported nanoparticles can present tremendous interests for catalytic applications for example.[3] Such structures can be obtained from conventional dry methods[4] or wet chemistries.[5] However, these processes generally require either high temperature syntheses or post-treatments like purification and drying steps, without ensuring good control on size and size distributions of the obtained nanomaterials. As an alternative, chemistry in supercritical fluids (SCFs) is of great interest as these media have unique tuneable properties intermediate between gas and liquid, which can be adjusted continuously by modulating temperature and/or pressure.[6]

Supercritical fluids have been successfully used to deposit either organic[7−11] or inorganic[12−16] materials. For example, high quality metallic films were deposited using supercritical fluid chemical deposition (SFCD) either on planar substrates,[17] particles,[14] or inside nanoporous templates.[18] The formation of surface nanostructures is achieved through the chemical transformation of metal-organic precursors in supercritical mixtures. The main interest of supercritical fluids is that high nucleation rates can be reached, compared with liquid phase syntheses, leading to narrow size distribution nanoparticles.[19] Previous works have been reported on supported nanoparticles synthesis like gold,[20] platinum,[21] ruthenium,[22] or copper ones.[13]

Authors have previously described a thermodynamic way to achieve control of the size.[21,23] Depending on the conditions in use, it is possible to tune the amount of metal-organic precursors adsorbed onto the surface of carbon nanotubes, or carbon aerogels, prior to their reduction. The transformation of this absorbed precursor by different ways (chemical reduction in a supercritical fluid with a reducing agent, chemical reduction with pure hydrogen at elevated temperature, thermal reduction in a supercritical fluid, thermal decomposition in an inert atmosphere, or chemical conversion with hydrogen or air at atmospheric pressure) is conducive to the formation of size controlled nanoparticles.

Another way to control the size of the deposited nano-objects includes controlling the kinetics of the precursor transformation. To achieve such a precise control, one can play not only on several operating parameters like temperature and residence time but also on the composition of reacting media. In the case of SFCD, supercritical CO_2 ($scCO_2$) is generally used as the main solvent, due to its low critical coordinates (T_c = 31.1 °C, P_c = 7.38 MPa). Most of the time, a cosolvent is added in order to improve the solubility of the precursor as well as to increase

* Corresponding author. E-mail: aymonier@icmcb-bordeaux.cnrs.fr.
[†] Institut de Chimie de la Matière Condensée de Bordeaux.
[‡] Université de Bordeaux.
[§] Université de Pau et des Pays de l'Adour.

10.1021/jp809533n CCC: $40.75
Published on Web 03/09/2009

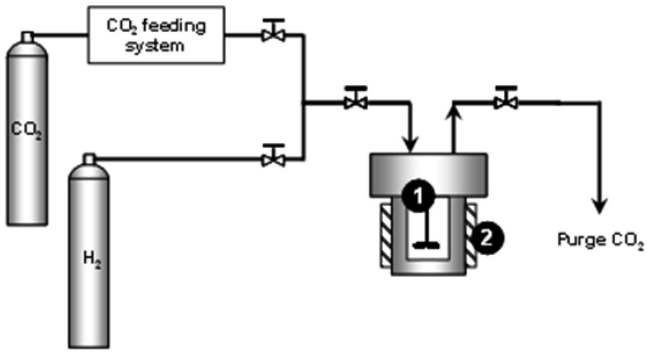

Figure 1. Experimental setup: (1) high pressure/high temperature stirred reactor, (2) heating element.

the overall density of the supercritical mixture. The nature of this cosolvent can strongly influence the kinetics of the metal-organic precursor transformation, as already shown in chemical vapor deposition processes. Indeed, it was reported that the use of alcohol cosolvents for reducing copper hexafluoroacetylacetonate hydrate $Cu(hfac)_2 \cdot H_2O$ with hydrogen[24,25] allows dramatic increases of the copper deposition rate.

In supercritical media, this effect was reported for the addition of ethanol (EtOH), allowing decreasing the decomposition temperature of roughly 30 °C.[26] In addition, other papers highlight that the use of hydrogen, added to this mixture as reducing agent, allows a softer chemical reaction, limiting the contamination of the deposited material by organic byproducts from the precursor.[27] We also demonstrated in a previous study that the reduction of $Cu(hfac)_2 \cdot H_2O$ in a supercritical CO_2/isopropanol/H_2 mixture in presence of silica spheres could lead to the formation of supported copper nanoparticles at relatively low temperature, with the size being controlled by tuning temperature and/or residence time,[13] demonstrating that the knowledge of the reaction kinetics is a key parameter.

On the basis of these considerations, this paper presents a kinetic way for controlling the size of supported metal nanoparticles. Starting from the literature results in vapor phase and in connection with the surface decoration process of silica spheres with nanoparticles, we have investigated the reduction kinetics of $Cu(hfac)_2 \cdot H_2O$ with H_2 in supercritical CO_2−alcohol media, successively using methanol (MeOH), ethanol (EtOH), and isopropanol (iPrOH). The kinetics were determined for low temperatures in the range 100−150 °C and residence time up to 120 min, at pressures ranging from 20 to 22 MPa. We report also in this paper for the first time on a model to predict the size of supported metal nanoparticles as a function of residence time and temperature.

2. Experimental Section

The reduction kinetics of $Cu(hfac)_2 \cdot H_2O$ with H_2 in supercritical CO_2/alcohol mixtures were determined by proportioning the remaining precursor after the reaction took place in a high pressure/high temperature experimental setup reported in Figure 1.

In a typical experiment, a high pressure high temperature stirred reactor of 50 cm^3 (1, Figure 1) is first loaded with an alcohol solution containing the precursor (0.05 mmol of $Cu(hfac)_2 \cdot H_2O$ in 0.05 mol of alcohol). It is thereafter pressurized with hydrogen (0.05 mol) and CO_2 (0.8 mol), using a feeding system composed of a chiller and a high pressure pump. The final molar composition of the reaction medium is CO_2/alcohol = 95/5 (initial pressure is 9 MPa at T = 25 °C). The mixture is stirred and heated to the desired conditions (100 °C < T < 150 °C) using an external heating element surrounding the reactor (2, Figure 1). A pressure sensor and a thermocouple, placed inside the reactor, allow following the experimental conditions. After a given residence time, the reactor is depressurized and the alcohol solution containing the remaining precursor is recovered for proportioning using UV−visible spectroscopy (Cary 1C UV−visible spectrophotometer apparatus).

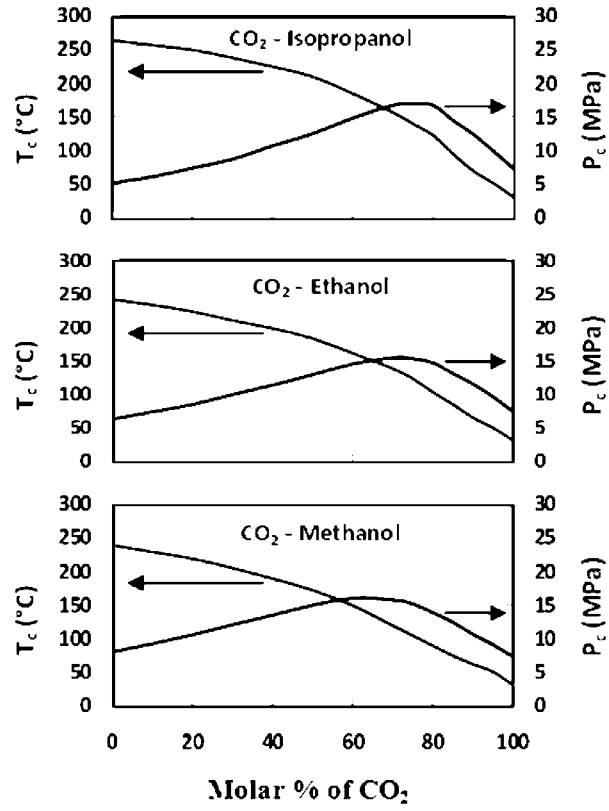

Figure 2. Evolution of the critical coordinates of CO_2/alcohol mixtures as a function of the molar percentage of CO_2 obtained with the PHOPHY software, using the EoS of Peng−Robinson.

$Cu(hfac)_2 \cdot H_2O$, methanol, ethanol, and isopropanol were purchased from Aldrich. CO_2 and H_2 were purchased from Air liquide and used as received.

The supercritical coordinates of the CO_2/alcohol mixtures versus the molar percentage of CO_2 were estimated by the equation of state (EoS) of Peng−Robinson (Figure 2). One can see that in the studied conditions (i.e., mixtures CO_2/alcohol: 95/5 molar, 100 °C < T < 150 °C and 20 MPa < P < 22 MPa), all three mixtures are under supercritical conditions.

The addition of H_2 can modify the critical coordinates of the system.[28] Taking into account these considerations, we have checked visually that the ternary mixtures CO_2/alcohol/H_2 were supercritical in the studied conditions by running experiments in a sapphire high pressure/high temperature reactor.

Preliminary UV−visible measurements were realized for each alcohol in order to determine the characteristic absorption band allowing following the precursor's concentration. As an example, Figure 3 presents UV−visible spectrum of $Cu(hfac)_2 \cdot H_2O$ in isopropanol for λ ranging from 210 to 360 nm after a chemical reduction was performed at 150 °C at different residence times. The two bands are attributed to ligand (π, π^*) transitions (λ = 307 nm with a shoulder at λ = 325 nm) and charge transfer between the ligand and the metallic

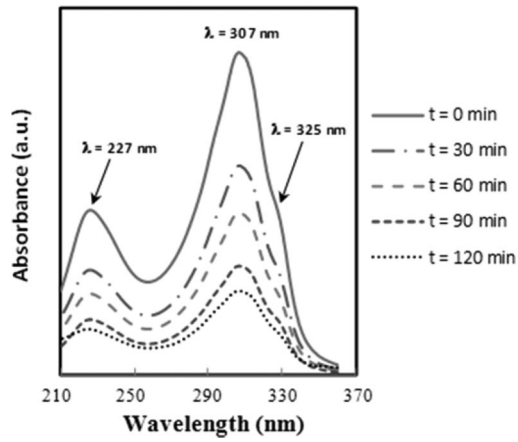

Figure 3. UV−visible absorption spectrum of $Cu(hfac)_2 \cdot H_2O$ in isopropanol after reduction at 150 °C for residence times ranging from 0 to 120 min.

center ($\lambda = 227$ nm), respectively.[29] By using a master curve verifying the Beer−Lambert's law, the concentrations were determined.

Several tests were performed with the different systems by varying the temperature (100−150 °C) and the residence time (0−120 min) in order to determine the reduction kinetics. The synthesis of silica-supported copper nanoparticles was performed for temperatures ranging from 100 to 125 °C by adding silica spheres in the reaction media. The mean sizes of the obtained copper nanoparticles were measured from TEM pictures. All of these data were integrated in a model developed to predict the evolution of the size of metal nanoparticles in the surface nanostructuration process.

3. Results and Discussion

3.1. Reduction Kinetics of $Cu(hfac)_2 \cdot H_2O$ with H_2 in CO_2/Alcohol Supercritical Media. From a general point of view, the reduction of $Cu(hfac)_2 \cdot H_2O$ to metal copper can be written as

$$Cu(hfac)_2 \cdot H_2O + H_2 + R{-}OH \rightarrow Cu^{(0)} + H_2O + 2\,H{-}hfac + R{-}OH \quad (1)$$

Since both alcohol and H_2 are in large excess compared with the precursor (molar ratio $= 10^3$), the order of the reaction with respect to these reactants is 0. The kinetics of disappearance of $Cu(hfac)_2 \cdot H_2O$ is given by eq 2:

$$\frac{d[Cu(hfac)_2 \cdot H_2O]}{dt} = -k_0 \exp\left(\frac{-E_a}{RT}\right) \cdot [Cu(hfac)_2 \cdot H_2O]^a \quad \text{with} \quad k_{app} = -k_0 \exp\left(\frac{-E_a}{RT}\right) \quad (2)$$

where k_0 is a constant, R is the perfect gas constant (8,314 $J \cdot K^{-1} \cdot mol^{-1}$), E_a is the activation energy of the reaction (in $J \cdot mol^{-1}$) and k_{app} is the appearing kinetic constant. From this equation, the k_{app} were determined at different temperatures. The proportioning of the precursor at the end of the experiment allows determining the conversion rate, defined as:

$$\text{conversion rate (CR)} = 1 - \frac{[Cu(hfac)_2 \cdot H_2O]_t}{[Cu(hfac)_2 \cdot H_2O]_{t=0}} \quad (3)$$

The conversion rates obtained within the framework of the study are reported in Figure 4.

These results were treated assuming a first order with respect to the precursor concentration. By integrating eq 2, we obtain

$$\text{Ln}([Cu(hfac)_2 \cdot H_2O]) = \text{Ln}([Cu(hfac)_2 \cdot H_2O]_{t=0}) - k_{app} \cdot t \quad (4)$$

Replacing the concentrations ratio by the conversion rate, it gives

$$\text{Ln}(1 - \text{CR}) = -k_{app} \cdot t \quad (5)$$

For each temperature and each alcohol cosolvent, Ln(1 − CR) was plotted as a function of the residence time (Figure 5).

These plots give straight lines, confirming the assumption of a first order reaction. The slopes correspond to the values of the rate constants, k_{app}, the values of which are presented in Table 1.

Depending on the alcohol used as cosolvent, the values of the rate constant can be tuned in the range $2 \cdot 10^{-4}$ min^{-1} − $3.2 \cdot 10^{-2}$ min^{-1} for low temperature ranging from 100 to 150 °C.

Using the obtained values of k_{app}, we can determine the activation energy of the reaction E_a, for each alcohol, by plotting the Napierian logarithm of k_{app} as a function of (1000)/(RT) (Figure 6).

The activation energy required to reduce $Cu(hfac)_2 \cdot H_2O$ is lower when MeOH is used as cosolvent (69 $kJ \cdot mol^{-1}$) compared with EtOH or iPrOH (80 $kJ \cdot mol^{-1}$ and 104 $kJ \cdot mol^{-1}$, respectively; Figure 6), showing that the nature of the alcohol strongly influences the value of the kinetics constant. First, the use of MeOH as cosolvent leads to larger values of k_{app} than EtOH or iPrOH (Table 1). One can also notice that the use of isopropanol, despite the low obtained kinetics (10^{-4} $min^{-1} < k_{app} < 10^{-2}$ min^{-1}), allows tuning the value of the kinetics constant over 2 orders of magnitude by adjusting the temperature in the range 100−150 °C, allowing obtaining a precise control over the reduction of $Cu(hfac)_2 \cdot H_2O$.

The variations of the copper deposition rate as a function of the alcohol used to assist the reduction of the precursor (iPrOH, EtOH, or MeOH) were reported equally in the case of the vapor phase processes. However, iPrOH leads to higher deposition rate than MeOH or EtOH.[30] The authors assume that this behavior is due to the pK_a value of these alcohols in water (pK_a iPrOH = 17.1, pK_a EtOH = 15.8, pK_a MeOH = 15.3), which depends directly on the ability of the alcohol to liberate a hydrogen atom and to assist the reduction. However, it has been shown that the tert-butanol, which should be even more efficient than the iPrOH, does not lead to higher copper deposition rate, since it is not able to complex the precursor, due to steric hindrance. Thus, according to these results, two main parameters have to be taken into account to choose the more efficient alcohol to assist the reduction of $Cu(hfac)_2 \cdot H_2O$. First, the alcohol has to be able to complex the precursor (sterically compatible). Then, the easier it is for the alcohol to liberate a hydrogen atom, the more efficient it will be to assist the reduction.

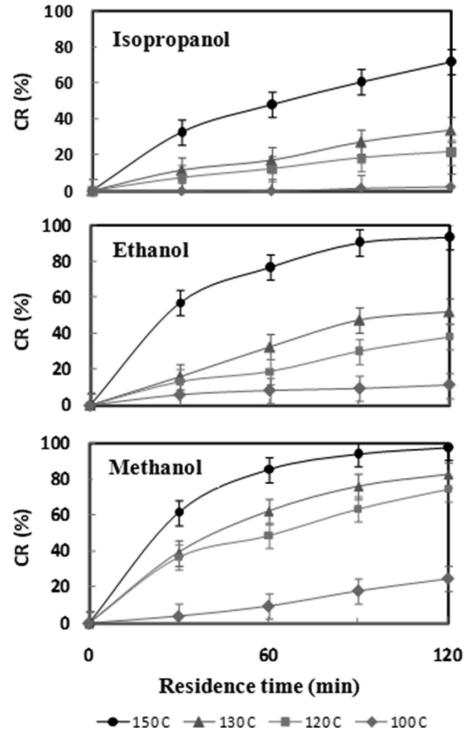

Figure 4. Conversion rates (CR, in %) of $Cu(hfac)_2 \cdot H_2O$, obtained for the different tests using methanol, ethanol, or isopropanol as cosolvent. Note that CR was not determined for iPrOH at $T = 100$ °C, $R_t = 30$ and 60 min, due to very low values.

TABLE 1: Kinetics Constants of the Reduction of $Cu(hfac)_2 \cdot H_2O$ with H_2 in Supercritical CO_2/Alcohol Media at Different Temperatures

T(°C)	k_{app} ($10^{-3} \cdot min^{-1}$)		
	MeOH	EtOH	iPrOH
100	2.2 ± 0.1	1.1 ± 0.3	0.2 ± 0.1
120	11 ± 0.8	4 ± 0.2	2.1 ± 0.1
130	15 ± 0.7	6.5 ± 0.5	3.1 ± 0.1
150	31 ± 1	24 ± 0.6	11 ± 0.4

These results and considerations are in contradiction with the kinetics that have been obtained in this study, using supercritical CO_2/alcohol mixtures. Thus, the reduction mechanisms proposed for the vapor phase reduction of $Cu(hfac)_2 \cdot H_2O$ by H_2 in presence of an alcohol are not valid anymore in supercritical media, mostly due to the presence of CO_2. To explain this behavior, it is required to study the interaction that can be developed inside the reaction media, in particular due to the presence of CO_2 molecules that constitute the main solvent. IR spectroscopy studies that were realized for supercritical CO_2/EtOH mixtures have shown that the alcohol molecules can interact with the CO_2 molecules. [31] Acceptor/donor bonds are created between the oxygen atom of the alcohol (which owns a negative charge: δ^-) and the carbon atom of the CO_2 molecule (which owns a positive charge: δ^+), as shown in Figure 7.

This mechanism was observed for all of the three alcohols studied in this work (MeOH, EtOH, and iPrOH). The complex that is mainly formed in our conditions (molar ratio CO_2/alcohol 95/5) is made of one CO_2 molecule for one alcohol molecule; however, some alcohol dimers have also been observed.[32] This complexation leads to a modification of the alcohol reactivity. First, it induces a steric hindrance surrounding the alcohol function, which will vary depending on the nature of the alcohol, so that it might not complex the copper precursor in the same way. Then, the charge distribution around the oxygen atom will vary inducing a modification of the hydrogen lability. These two phenomena can explain the different behaviors observed in vapor phase deposition and in supercritical fluid chemical deposition.

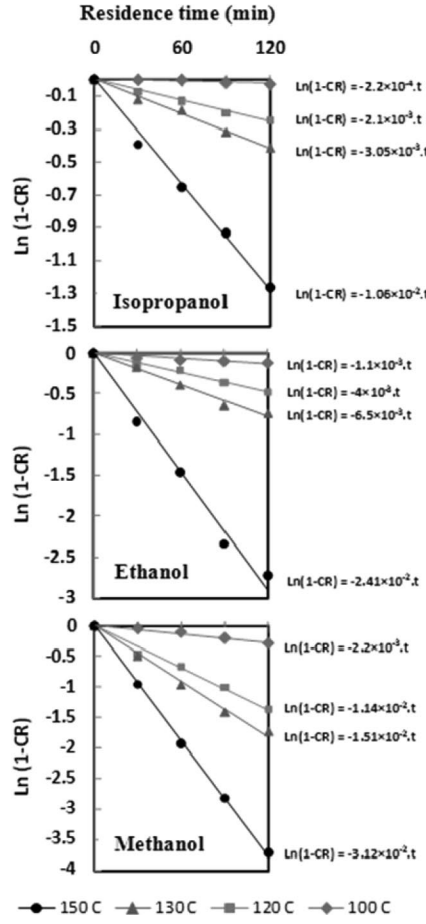

Figure 5. Ln(1 − CR) as a function of the residence time for the reductions performed using successively methanol, ethanol, and isopropanol as cosolvent at different temperatures.

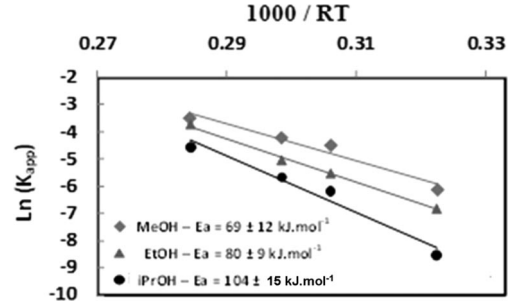

Figure 6. Evolution of the Napierian logarithm of k_{app} as a function of $1000/RT$ and deduced value of the activation energy for each of the three alcohols.

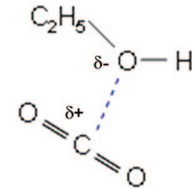

Figure 7. Representation of the donor−acceptor interaction between a CO_2 and an ethanol molecule.

Starting from these results, we have chosen to use CO_2/iPrOH supercritical mixtures to decorate the surface of silica spheres

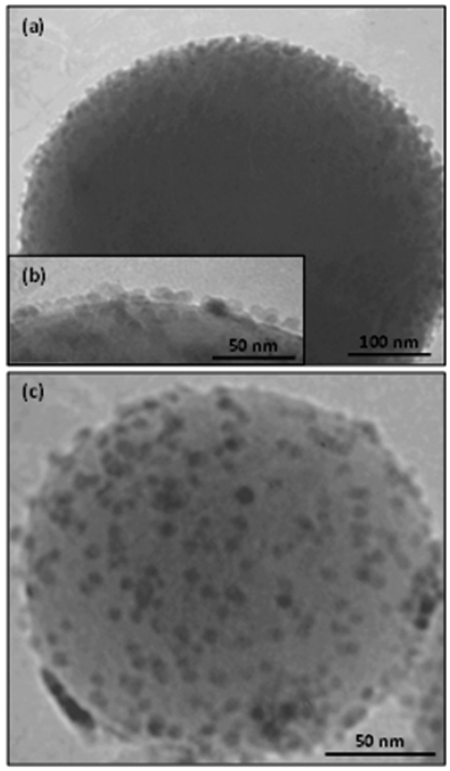

Figure 8. (a) TEM pictures of a 500 nm silica sphere decorated by copper nanoparticles using the reduction of $Cu(hfac)_2 \cdot H_2O$ with H_2 in supercritical CO_2/iPrOH media. (b) Enlargement of a. (c) TEM pictures of a 170 nm silica sphere decorated by copper nanoparticles.

TABLE 2: Experimental Conditions and Mean Diameter of the Copper Nanoparticles Measured from TEM Pictures

sample	operating conditions		particle diameter d_{avg} (nm)	
	P (MPa)	T (°C)	R_t[a] (min)	
1	20	100	60	5 ± 2
$m_{precursor}$[b] $= 25.6$ mg			90	6 ± 3
μ_f [c] $= 3.33.10^{-5}$ Pa·s			120	9 ± 5
ρ_f [d] $= 525$ kg·m^{-3}				
2	22	115	60	10 ± 5
$m_{precursor} = 25.6$ mg			90	12 ± 5
$\mu_f = 3.49.10^{-5}$ Pa·s			120	16 ± 6
$\rho_f = 498$ kg·m^{-3}				
3	23	125	60	11 ± 5
$m_{precursor} = 25.6$ mg			90	14 ± 6
$\mu_f = 3.5.10^{-5}$ Pa·s			120	17 ± 5
$\rho_f = 460$ kg·m^{-3}				

[a] R_t is the residence time. [b] $m_{precursor}$ is the weigth of $Cu(hfac)_2 \cdot H_20$ introduced in the reaction media. [c] μ_f is the viscosity of the media. [d] ρ_f is the density of the media.

with copper nanoparticles by reducing $Cu(hfac)_2 \cdot H_2O$ with H_2. This choice is supported by the fact that iPrOH, as a cosolvent, allows tuning the value of the kinetics constant over 2 orders of magnitude by adjusting the temperature in the range 100−150 °C. This mastering of the kinetics allows controlling precisely the nucleation rate, which is an important parameter for the design of supported nanostructures.

3.2. Synthesis of Silica Spheres Decorated with Copper Nanoparticles at Low Temperature. On the basis of the results obtained from the kinetics measurements, silica spheres (170 and 550 nm in diameter) dispersed in the reactive media were decorated by copper nanoparticles by reducing $Cu(hfac)_2 \cdot H_20$ with H_2 in supercritical CO_2/iPrOH mixtures (95/5 molar) by varying temperature and residence time.

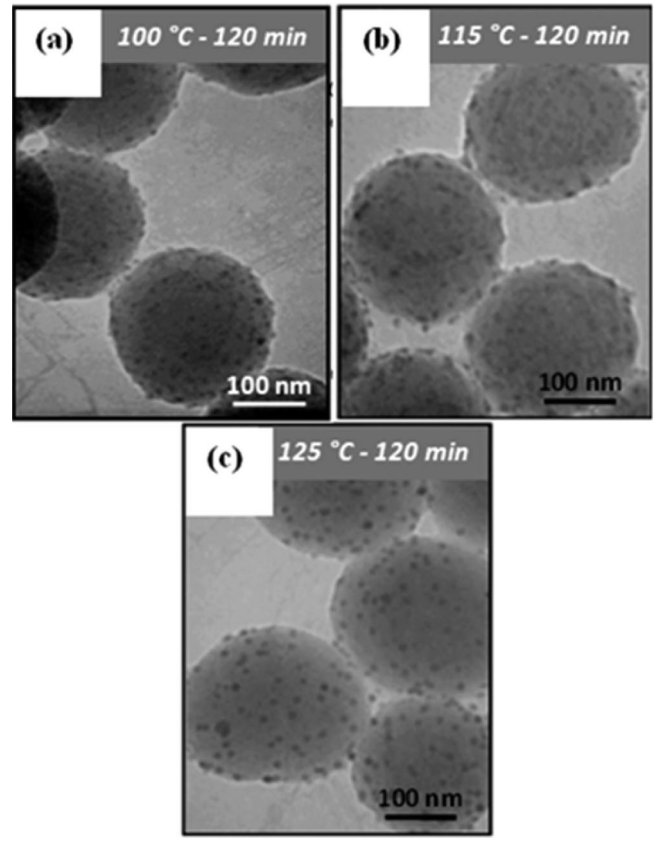

Figure 9. Silica particles decorated with copper nanoparticles at $R_t = 120$ min and $T = 100$ °C (a), $T = 115$ °C (b), and $T = 125$ °C (c).

Figure 8a presents a typical TEM picture of silica@nanoCu nanocomposite. The copper nanoparticles have a conventional spherical shape corresponding to the minimization of the surface energy and form a monolayer on the surface of the silica spheres (Figure 8b).

In order to quantify the influence of the reduction kinetics of the precursor on the eventual size of the supported nanoparticles, copper nanoparticles were deposited on 170 nm silica particles (for better visualization), and their sizes were measured from TEM pictures by manual counting (Figure 8c). The change in size for the silica spheres does not affect the sizes of the copper nanoparticles; however, lower rates of coverage of the surface were observed because of higher available specific surface area for the smaller silica spheres. The results and experimental conditions are summarized in Table 2. The fluid properties were estimated either using the Reichenberg correlation, which is known to be valid for the high pressure fluids (for viscosity) or using the EoS of Peng−Robinson (for the density).

By tuning temperature (100−125 °C) and/or residence time (60−120 min), we are able to tune the size of the copper nanoparticles (d_{avg}) from 5 to 17 nm, as shown in Table 2. As an example, Figure 9a−c shows the effect of temperature on the size of copper nanoparticles synthesized at $R_t = 120$ min, $T = 100$, 115, and 125 °C, respectively.

The evolution of d_{avg} as a function of R_t and T for the obtained copper nanoparticles can be directly linked to the values of the kinetics constants, showing a kinetically controlled formation of the supported nanoparticles.

According to these experimental results, we have developed a model to describe the surface decoration of materials by metal nanoparticles.

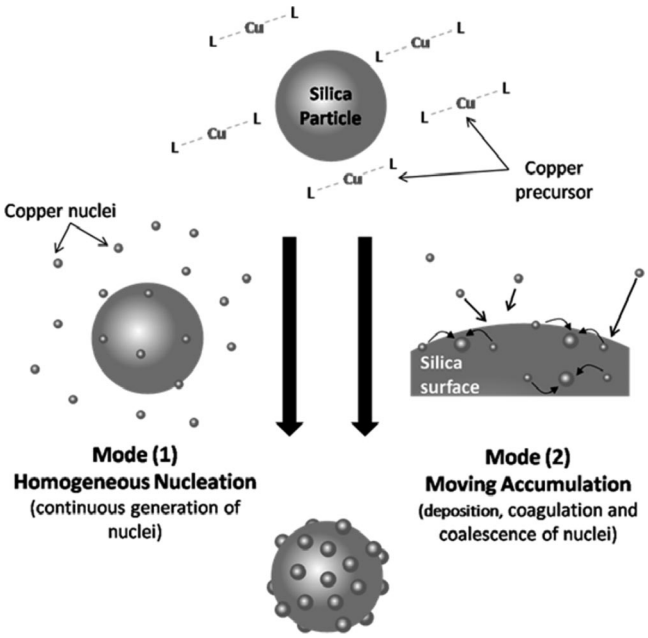

Figure 10. Schematic representation of the two modes of the bimodal model developed to predict the size of supported nanoparticles.

3.3. Modeling of the Deposition Process. ***The Bimodal Model.*** In a general way, the evolution of a particle size distribution can be described by a partial differential equation named the aerosol general dynamic equation.[33] This equation is used for simultaneous aerosol nucleation, condensation, coalescence, and coagulation. Different methods are usually used to solve this kind of equation. First, the sectional method, with either fixed or moved sections[34] is very efficient but the computational time is important. Then, the method of moments,[35] assuming that the shape of the distribution is log-normal or monodisperse, allows simplifying the partial differential equation into a set of ordinary differential equations preserving the most important information about the process and for a computational time much shorter than the sectional methods. A simple monodisperse model derived from the moment method[36] has been proposed to predict particle size distribution. The phenomena taken into account for the growth of particles were coalescence and aggregation. The results fit well with those obtained by the rigorous sectional method. This model was successfully applied to material synthesis in high temperature gases,[37] as well as to the synthesis of metal nanoparticles in supercritical fluids with instantaneous precursor decomposition.[38] However, for nonsimultaneous precursor decomposition, as discussed in this paper, this monodisperse model leads to erroneous results for the particle size distribution.

In this context, we have used a bimodal model[39] to predict the evolution of the mean size of the supported copper nanoparticles as a function of R_t and T. This model takes into account the coalescence and the aggregation mechanisms and is well suited in the case of very low precursor decomposition rates. The bimodal model is in very good agreement with the complete sectional model and requires the same level of computation time that the simple monodisperse model. This model is composed of two discrete monodisperse modes used to represent the particle size distribution: a size fixed nucleation mode (mode 1) and a moving accumulation mode (mode 2; Figure 10). The size fixed nucleation mode accounts for the introduction of newly generated particles (i.e., the generation of nuclei due to the precursor decomposition), and the moving accumulation mode characterizes the particle growth by coagulation and coalescence.

The model allows the description of the particle size evolution by the variation of four variables: the nuclei volume concentration of mode 1 N_1, the particle volume concentration of mode 2 N_2, the volumetric concentration of the aggregates V_2, and the particle surface area concentration of mode 2 A_2. In the model, the average volume of mode 2 is r times larger than v_0, and r increases following the growth of aggregate particles by coagulation and coalescence. The volume of the nuclei in mode 1 v_0 is assumed to be constant and fixed to the volume of a copper atom. The obtaining of the following set of eqs 6−9 is detailed elsewhere.[38]

The governing equation for N_1 is given by

$$\frac{dN_1}{dt} = -\frac{1}{2}\beta_{11}N_1^2\left(\frac{r}{r-1}\right) - \beta_{12}N_1N_2 + I \qquad (6)$$

where β_{11} and β_{12} represent respectively the intramode coagulation kernel in mode 1 and the intermode coagulation kernel between modes 1 and 2. The rate of particle formation I, depending on precursor's reduction kinetics, is calculated by the relation

$$I = N_a\frac{m_p}{M_p}k_{app}\exp(-k_{app}t) \qquad (7)$$

with N_a the Avogadro number, m_p and M_p the mass of the precursor and the molar mass of the precursor, respectively, and k_{app} the constant kinetic estimated in the previous section.

In the same way, the evolution of N_2 and V_2 is given by the following equations:

$$\frac{dN_2}{dt} = -\frac{1}{2}\beta_{11}N_1^2\left(\frac{1}{r-1}\right) - \frac{1}{2}\beta_{22}N_2N_2 \qquad (8)$$

$$\frac{dV_2}{dt} = -\frac{1}{2}\beta_{11}N_1^2\left(\frac{r}{r-1}\right)v_0 + \beta_{12}N_1N_2v_0 \qquad (9)$$

where β_{22} represents the intramode coagulation in mode 2.

The particle surface area concentration of mode 2 A_2 increases by intermode coagulation and decreases by intramode coagulation in mode 1 and by coalescence (third term on the right-hand side), so the evolution of A_2 is given by

$$\frac{dA_2}{dt} = -\frac{1}{2}\beta_{11}N_1^2\left(\frac{r}{r-1}\right)a_0 + \beta_{12}N_1N_2a_0 - \frac{1}{\tau_f}(A_2 - N_2a_{2s}) \qquad (10)$$

where τ_f is the characteristic sintering time and a_{2s} is the surface area of the completely fused (spherical) aggregate consisting of 2 particles. Note that only the particles in mode 2 are affected by coalescence; indeed, the particles in mode 1 are assumed to be spherical with a constant volume v_0.

Definition of Parameters. For each aggregate in modes 1 and 2, the volume and surface area are described by the relations

$$V_2 = N_2v_2, A_2 = N_2a_2 \qquad (11)$$

$$V_1 = N_1 v_0, A_1 = N_1 a_0 \tag{12}$$

with v_0 and a_0 the fixed volume and surface area of the monomer, respectively. v_2 and a_2 are the volume and surface area of the aggregate, respectively.

The primary particle size d_{p2} and the number of primary particles n_{p2} in an aggregate are defined by

$$d_{p2} = \frac{6V_2}{A_2} \tag{13}$$

$$n_{p2} = \frac{6V_2}{\pi d_{p2}^3} \tag{14}$$

The surface area of the completely fused (spherical) aggregate a_{2s} consisting of two particles is calculated by

$$a_{2s} = \pi 2^{2/3} d_p^2 \tag{15}$$

Coagulation Kernel. For the calculation of the coagulation kernel in mode 2, the collision diameter d_{c2} is preferred to the primary particle diameter d_{p2} in order to take into account the fractal-like aggregates (i.e., nonspherical aggregates). The collisions radius is defined by[40]

$$d_{c2} = d_{p2}\left(\frac{V_2}{v_{p2}}\right)^{1/D_f} = d_{p2}(n_{p2})^{1/D_f} = \frac{3V_2}{a_2}\left(\frac{a_2^3}{36\pi V_2^2}\right)^{1/D_f} \tag{16}$$

with D_f the fractal dimension. The value of the fractal dimension is generally fixed to 1.8 for cluster−cluster aggregation in the free molecule and continuum regime.[21,41] The collision radius in mode 1 is the particle diameter ($d_{c1} = d_{p1}$).

The collisions diameter is used to replace the solid sphere radius in the Fuchs interpolation expression for Brownian coagulation in the free molecule and continuum regimes.[42] So, the collision frequency is given by the relation

$$\beta_{ij} = 2\pi(D_i + D_j)(d_{ci} + d_{cj})\left[\frac{d_{ci} + d_{cj}}{d_{ci} + d_{cj} + 2g_{ij}} + \frac{8(D_i + D_j)}{c_{ij}(d_{ci} + d_{cj})}\right]^{-1} \tag{17}$$

where the particle diffusion coefficient D_i is calculated from the Stokes−Einstein expression with a Cunningham slip correction factor: [43]

$$D_i = \frac{k_b T}{3\pi\mu_f d_{ci}}\left[\frac{5 + 4Kn_i + 6Kn_i^2 + 18Kn_i^3}{5 - Kn_i + (8 + \pi)Kn_i^2}\right] \text{for i} = 1,2 \tag{18}$$

with the Knudsen number Kn_i as the ratio of the mean free path in the fluid λ_g over the particle radius diameter d_{pi} defined by

$$Kn_i = \frac{2\lambda_f}{d_{ci}} = \frac{2}{d_{ci}}\left(\frac{\pi}{\rho_f}\sqrt{\frac{\pi M_f}{2RT}}\right) \text{for i} = 1,2 \tag{19}$$

where ρ_f, μ_f, and M_f are respectively the density, the viscosity, and the molar mass of the fluid.

The mean particle speed c_{12} and the transition parameter g_{12} are given by

$$c_{12} = (c_1^2 + c_2^2)^{1/2}$$

$$c_i = \sqrt{\frac{8k_b T}{\pi\rho_p V_i}} \quad \text{for} \quad i = 1,2 \tag{20}$$

$$g_{12} = (g_1^2 + g_2^2)^{1/2}$$

$$g_i = \frac{1}{3d_{ci}l_i}[(d_{ci} + l_i)^3 - (d_{ci}^2 + l^2)^{3/2}] - d_{ci} \quad \text{for} \quad i = 1,2 \tag{21}$$

where l_i is the particle mean free path defined by,

$$l_i = \frac{8D_i}{\pi c_i} \tag{22}$$

Characteristic Sintering Time. The characteristic coalescence time is an important parameter. For nanomaterials, the coalescence process is highly influenced by the particle size and the temperature. As discussed elsewhere,[44] the dominant coalescence mechanism which prevails for nanoparticles seems to be the surface diffusion. The coalescence time for surface diffusion can be estimated by[45]

$$\tau = \frac{r_p^4}{b(T)} \tag{23}$$

with

$$b(T) = \frac{225\delta D_s \sigma M}{\rho_p RT} \tag{24}$$

where D_s is the surface diffusion coefficient, σ is the surface tension, and δ is the surface layer thickness. Unfortunately, the estimation of the physical parameters, for the range of nanomaterials, is very difficult.

Another approach is to use the experimental data with the simulation in order to adjust the coalescence parameters. We propose to define the characteristic coalescence time by the expression

$$\tau = k_0 r_p^4 \frac{T}{T_0}\exp\left(\frac{E_a}{R}\left(\frac{1}{T} - \frac{1}{T_0}\right)\right) \tag{25}$$

The pre-exponential term k_0 and the activation energy E_a were estimated previously[38] for copper materials synthesis considering an instantaneous decomposition of the precursor:

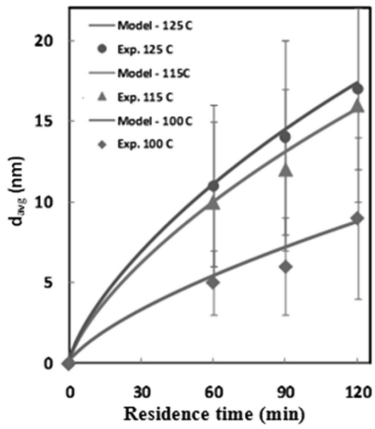

Figure 11. Evolution of copper primary particle size versus residence time.

$$k_0 = 11 \pm 5 \cdot 10^{31}\ \mathrm{m^{-4}s}$$

$$E_a = 20 \pm 5\ \mathrm{kJ \cdot mol^{-1}}$$

Simulation. The model was compared to the experimental results concerning the formation of metal copper particles on the surface of silica spheres in supercritical CO_2/iPrOH mixture (90/5 molar ratio; from Table 2). Additional data concerning copper (i.e., $M(Cu(hfac)_2 \cdot H_2O = 495.6\ g \cdot mol^{-1}$, $M(Cu) = 63.5\ g \cdot mol^{-1}$, $\rho(Cu) = 8.9\ g \cdot mL^{-1}$, diameter of a copper atom = 2.8 Å) were obtained from literature to make the calculation. The resolution of the system (eqs 6−9) is achieved with the RADAU5 subroutine (Implicit Runge−Kutta method of order 5), developed by Hairer,[46] which is particularly well-suited for the stiff problem.

Figure 11 represents the evolution of the primary copper particle size as a function of residence time and temperature.

A good agreement is obtained between experimental and calculated primary particle size for the model including both the coalescence and the aggregation mechanisms taken into account. The proposed mechanism for the silica sphere decoration process (i.e., homogeneous nucleation followed by heterogeneous growth) is confirmed in the studied conditions. However, it might not be suitable anymore for unexplored conditions, in particular, for temperatures above 150−175 °C, where there is a competition between two decomposition processes of the precursor (reduction by H_2/alcohol and thermolysis). This would indeed change the decomposition kinetics and thus the parameters of the model.

In the studied conditions, the first mode (homogeneous nucleation in the reaction media) is the limiting step of the process, which control the number of nuclei released in the reaction media. Since this is directly dependent on the precursor transformation kinetics, these model results clearly show the surface decoration of materials is a kinetically controlled process.

4. Conclusion

We have demonstrated the alcohol-assisted decoration of silica spheres by copper nanoparticles with a kinetic control of the copper nanoparticle size. This is achieved at low temperature (100−125 °C) using isopropanol as cosolvent, which allows tuning the reduction kinetics of the precursor over 2 orders of magnitude ($k = 2.2 \cdot 10^{-4}\ \mathrm{min^{-1}} - 1.1 \cdot 10^{-2}\ \mathrm{min^{-1}}$) compared with using methanol or ethanol. A bimodal model was used to predict the size of the obtained copper nanoparticles. This takes into account both the introduction of newly generated nuclei from the precursor decomposition and the particle growth on the surface of the silica spheres by coagulation and coalescence. This model, developed for low temperature decomposition of the precursor, fits well with the experimental data obtained and can be applied to other kinds of material nanostructurations. This work demonstrates a new way for controling the size of supported nanoparticles, which is an important parameter for applications like catalysis, where the specific surface is a critical factor.

Acknowledgment. Financial support from the French National Research Agency (ANR) is gratefully acknowledged (Project NANO4F). ICMCB is a member of the PILA network for high research and technological resources in multidisciplinary actions. The authors also want to thank Dr. Ryan Hartman for the interest he had shown in this work.

References and Notes

(1) Rotello, V. M. *Nanoparticles: building block for nanotechnology*; Springer: New York, 2003.
(2) (a) Rieter, W. J.; Taylor, K. M. L.; Lin, W. *J. Am. Chem. Soc.* **2007**, *129*, 9852–9853. (b) Rampazzo, E.; Brasola, E.; Marcuz, S.; Mancin, F.; Tecilla, P.; Tonellato, U. *J. Mater. Chem.* **2005**, *15*, 2687–2696.
(3) (a) Volbaek, B. H.; Janssens, T. V. W.; Clausen, B. S.; Falsig, H.; Christensen, C. H.; Norskov, B. S. *Nanotoday* **2007**, *2* (4), 14–18. (b) Astruc, D. *Nanoparticles and catalysis*; Wiley: New York, 2007.
(4) Luo, J.; Luo, R.; Zhang, W. *Chem. Vap. Dep.* **2007**, *13*, 574–580.
(5) Shi, W.; Sahoo, Y.; Swithart, M.; Prasad, P. *Langmuir* **2005**, *21*, 1610–1617.
(6) Eckert, C.; Knutson, B. L.; Debenedetti, P. G. *Nature* **1996**, *383*, 313–318.
(7) Reverchon, E.; Adami, R. J. *Supercritical Fluids* **2006**, *37*, 1–22.
(8) Reverchon, E. J. *Supercritical Fluids* **1999**, *15*, 1–21.
(9) Jung, J.; Perrut, M. J. *Supercritical Fluids* **2001**, *20*, 179–219.
(10) Shariati, A.; Peters, C. *Curr. Opin. Solid State Mater. Sci.* **2003**, *7*, 371–383.
(11) Marre, S.; Cansell, F.; Aymonier, C. *Langmuir* **2008**, *24*, 252–258.
(12) (a) Aymonier, C.; Loppinet-Serani, A.; Reveron, H.; Garrabos, Y.; Cansell, F. J. *Supercritical Fluids* **2006**, *38* (2), 242–251. (b) Cansell, F.; Aymonier, C J. *Supercritical Fluids* **2009**, *47* (3), 508–516.
(13) Marre, S.; Cansell, F.; Aymonier, C. *Nanotechnology* **2006**, *17*, 4594–4599.
(14) Pessey, V.; Garriga, R.; Weill, F.; Chevalier, B.; Etourneau, J.; Cansell, F. *Ind. Eng. Chem. Res.* **2000**, *39* (12), 4714–4719.
(15) Cansell, F.; Aymonier, C.; Loppinet-Serani, A. *Curr. Opin. Solid State Mater. Sci.* **2003**, *7*, 331–340.
(16) Aymonier, C.; Elissalde, C.; Reveron, H.; Weill, F.; Maglione, M.; Cansell, F. J. *Nanosci. Nanotech.* **2005**, *5* (6), 980–983.
(17) Blackburn, J. M.; Long, D. P.; Cabañas, A.; Watkins, J. *Science* **2001**, *294*, 141–145.
(18) O'Neil, A. *Watkins, MRS Bull.* **2005**, *30*, 967–975.
(19) Marre, S.; Park, J.; Rempel, J.; Guan, J.; Bawendi, M. G.; Jensen, K. F. Adv. Mater. **2009**, *20* (24), 4830–4834.
(20) Zhang, Y.; Erkey, C. *J. Supercrit. Fluids* **2006**, *38* (2), 252–267.
(21) Bayrakceken, A.; Kitkamthorn, U.; Aindow, M.; Erkey, C. *Scripta Materialia* **2007**, *56*, 101–103.
(22) Zhang, Y.; Kang, D.; Aindow, M.; Erkey, C. *J. Phys. Chem. B* **2005**, *109* (7), 2617–2624.
(23) Zhang, Y.; Cangul, B.; Garrabos, Y.; Erkey, C. *J. Supercrit. Fluids* **2008**, *44* (1), 71–77.
(24) Chiang, C.; Miller, T.; Dubois, L. *J. Phys. Chem.* **1993**, *97*, 11781–11786.
(25) Jain, A.; Kodas, T.; Corbitt, T.; Hampden-Smith, M. *Chem. Mater.* **1996**, *8*, 1119–1127.
(26) M'Hamdi, R.; Bocquet, J.; Chfor, K.; Pommier, C. *J. Supercrit. Fluids* **1991**, *4*, 55–59.
(27) Kondoh, E.; Kato, H. *Microelec. Eng.* **2004**, *64*, 495–499.
(28) Ke, J.; Han, B.; George, M. W.; Yan, H.; Poliakoff, M. *J. Am. Chem. Soc.* **2001**, *123*, 3661–3670.
(29) Lussier, L.; Sandorfy, C.; Goursot, A.; Penigault, E.; Weber, J. *J. Phys. Chem.* **1984**, *88*, 5492.
(30) Borgharkar, N.; Griffin, G.; James, A.; Maverick, A. *Thin Solid Films* **1998**, *320*, 86–94.
(31) (a) Cabaço, M.; Danten, Y.; Tassaing, T.; Longelin, S.; Besnard, M. *Chem. Phys. Lett.* **2005**, *413*, 258–262. (b) Lalanne, P.; Tassaing, T.; Danten, Y.; Cansell, F.; Tucker, S.; Besnard, M. *J. Phys. Chem. A* **2004**, *108*, 2617–2624. (c) Besnard, M.; Tassaing, T.; Danten, Y.; Andanson, J. M.;

Soetens, J. C.; Cansell, F.; Loppinet-Serani, A.; Reveron, H.; Aymonier, C. *J. Mol. Liq.* **2006**, *125*, 88–99.

(32) Fulton, J.; Yee, G.; Smith, R. *Supercritical fluid engineering science: Fundamental and applications*; Kiran, E., Brennecke, J., Eds.; Washington DC, 1993, *514*, 175.

(33) Frieldlander, S. K. *Smoke, Dust, and Haze*, 2nd edition; Oxford University Press: Oxford, England, 2000.

(34) Hounslow, M. J.; Ryall, R. L.; Marshall, V. R. *AIChE J.* **1988**, *34*, 1821–1832.

(35) (a) Randolph, A. D.; Larson, M. A. *Theory of particulate systems*; Academic Press: New York, 1971. (b) Pratsinis, S.E. J. *Colloid Interface Sci.* **1988**, *124* (2), 416–427.

(36) Kruis, F. E.; Kusters, K. A.; Pratsinis, S. E.; Scarlett, B. *Aerosol Sci. Technol.* **1993**, *19*, 514–526.

(37) (a) Johannessen, T.; Pratsinis, S. E.; Livbjerk, H. *Chem. Eng. Sci.* **2000**, *55*, 177–191. (b) Schild, A.; Gutsch, A.; Muhlenweg, H.; Pratsinis, S. E. *J. Nanoparticle Res.* **1999**, *1*, 305–315. (c) Tsantilis, S.; Kammler, H. K.; Pratsinis, S. E. *Chem. Eng. Sci.* **2002**, *57*, 2139–2156.

(38) Erriguible, A.; Marias, F.; Cansell, F.; Aymonier, A. J. Supercritical Fluids, 2008, DOI: 10.1016/j.supflu.2008.09.014.

(39) Jeong, J. I.; Choi, M. *J. Aerosol Sci.* **2003**, *34*, 965–976.

(40) Matsoukas, T.; Friedlander, S.K. *J. Colloid Interface Sci.* **1991**, *146*, 495–506.

(41) Kaplan, C. R. *Aerosol Sci. Technol.* **1988**, *8*, 11–28.

(42) Seinfeld, J. H. *Atmospheric Chemistry and Physics of Air Pollution*; John Wiley & Sons: New York, 1986.

(43) Phillips, W. F. *Phys. Fluids* **1975**, *1*, 1089–1093.

(44) Johannessen, T. *Synthesis of nano-particles in flames, PhD Thesis*, Technical University of Denmark, 1999.

(45) Lehtinen, K. E. *Theoretical studies on aerosol agglomeration processes, PhD Thesis*, VTT Technical Research Centre of Finland, 1997.

(46) Hairer, E.; Wanner, G. *Springer Series in Comput. Mathematics, 14*, Springer-Verlag 1991, Second revised edition, 1996.

JP809533N